Window strategies for moving objects

F. Mignard, P. Tanga
Observatoire de la Côte d'Azur
Dpt. Cassiopée

GAIA-CH-TN-OCA-FM-024-02

09 May 2006

Abstract

In this note we show the peculiarities of the observations of the solar system objects with Gaia and propose several alternatives in the window scheme to optimise the observation strategy to maximise the science return. While some proposals are unrealistic at this stage of advancement of the design, the requests and wishes given in the conclusion should be seriously considered for an implementation.

1 Introduction

The observation of solar system objects is a very challenging objective for Gaia and the involved science ranks very high in the Gaia proposal. Regarding the Solar System science astrometric and photometric observations are the main targets, but the possibility to calibrate the RVS spectra with asteroids (where both the spectra and the radial velocities are well known) is actively investigated and promising [1].

Due to their motion and their size they present specific problems in data handling during the crossing of the focal plane. As a result of their intrinsic displacement on the sky they will drift inside the acquisition window to such an extent that they may be lost before the end of the transit, leading to a serious loss of astrometric and/or photometric data if not properly handled. The exact level of loss is assessed for the

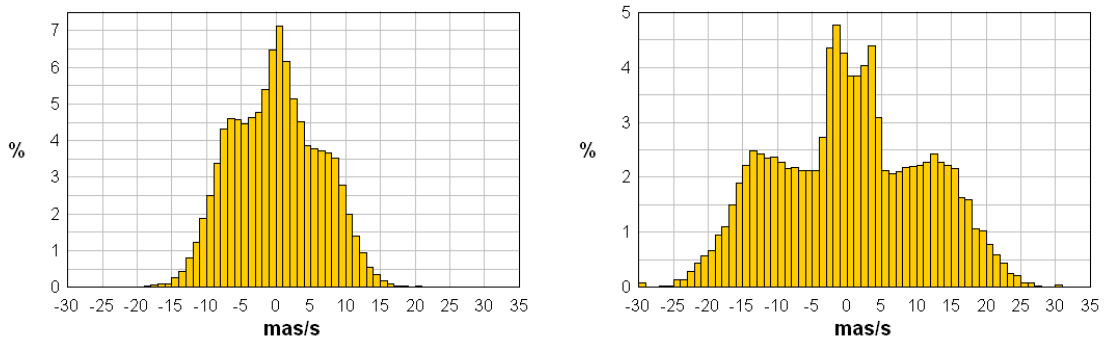


Figure 1: Statistical distribution of the proper velocity of main belt asteroids when they are observed by Gaia. The plots give the distributions of the along-scan velocity (left) and across-scan velocity (right) in mas/s during the crossing of one of the Gaia FOVs. The plots are based on the solar system simulation run over the first 20,000 numbered asteroids.

nominal window scheme using realistic representation of the transit velocity for the main belt objects (MBO) and the near Earth objects (NEO). If a solution is found for the MBO it will be also applicable without change to the minor planets orbiting at larger distances, like the Trojans and the Kuiper belt objects. The problem of their size is much less serious, but at least for the few hundreds largest, this will smear significantly the PSF and degrade the astrometric precision. On the other hand, both the size and shape of the largest objects will be determined by comparing the actual signal to the PSF.

With a limiting visual magnitude of 20 mag it is estimated that about 500,000 objects, primarily from the main belt, will be observed by Gaia. From the annual growth of the discovery one can guess that Gaia will find about 100,000 new objects, for which no initial orbit will be available. Most of the objects to be observed will fall close the limiting magnitude between V= 19 and 20. Therefore in the following the window parameters are those pertaining to faint objects. About 200 hundreds among the sources will have an angular size > 50 mas during the transit in the Gaia field of views and their size and shape will be investigated from the departure of the signal from the nominal PSF.

2 The major issues

2.1 Inertial velocity of solar system bodies

For the following it is important to have in mind the typical magnitude of the inertial velocity of solar system bodies together with the statistical distribution showing what proportion of a given category have a velocity less than a specified velocity. The following plots of the AL and AC velocity distributions are constructed from the simulation of the passage of minor planets in the fields of view of Gaia. The first 20,000 numbered asteroids are used and this set comprises primarily main belt objets. Therefore the results are fully representative of what we expect for the vast majority of the sources Gaia will observe. The overall distributions are shown in Fig. 1 for the along and across-scan velocity expressed in mas/s. There is a significant difference between the two directions : the typical velocity (meaning its absolute value) is around 7 mas/s Al and 11 mas/s AC. However the two distributions are not independent since the speed plotted in Fig. 2 is never very small. If the AL projection is small this means in general that the actual motion is perpendicular to the scanning direction and that the AC speed tends to be large.

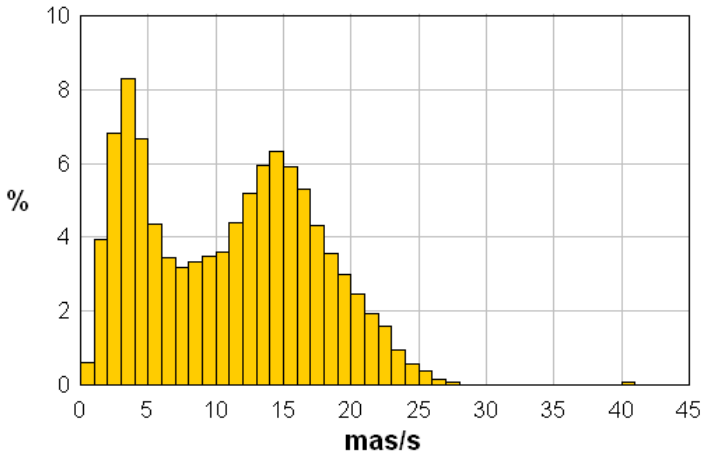


Figure 2: Statistical distribution of the proper speed of main belt asteroids when they are observed by Gaia. The plots give the modulus of the velocity vector in mas/s during a FOV crossing.

The distributions of the projected velocities or of the speed are clearly not unimodal (this is obvious for the speed in Fig. 2 with one population of small velocity of few mas/s and a larger one at about 15 mas/s) although the population of the

minor bodies is rather uniform, with more than 90% of the planet having a semi-major axis between 1.9 and 3.2 au. This must come from the observation geometry which favours observations at specific solar elongation. Much of the observations are clumped in two directions, namely solar elongation of 180 - 45 = 135 degrees, and another almost symmetrical peak at 45 degrees. The distance to the Earth is small in the first case ($\sim$ 2 au) and large in the second ($\sim$ 3 au) and one would expect the angular velocities to be in direct relation with these distances : small (resp. large) elongations should yield small (resp. large) velocities. What happens is just this opposite of this apparently sound conclusion, because the elongation of 135 degrees is very close to the stationary point when the apparent motion of a standard main belt asteroid starts being retrograde. Therefore one has much larger velocities for small elongations and very small velocities for the observations taking place near the maximum possible elongations. This is shown in Fig. 3 for the along-scan velocity with the small elongations on the left plots and the large ones on the right and similarly in Fig. 5 for the across scan velocities. The proportions of observations in the two directions are not equal because the time spent by a planet in the vicinity of each extreme elongation is not the same. In addition more source get fainter than $G = 20$ at small elongations since the average distance to the Earth is larger. For the whole population a correct weighting is close to 55% for small elongations and 45% for large elongations.

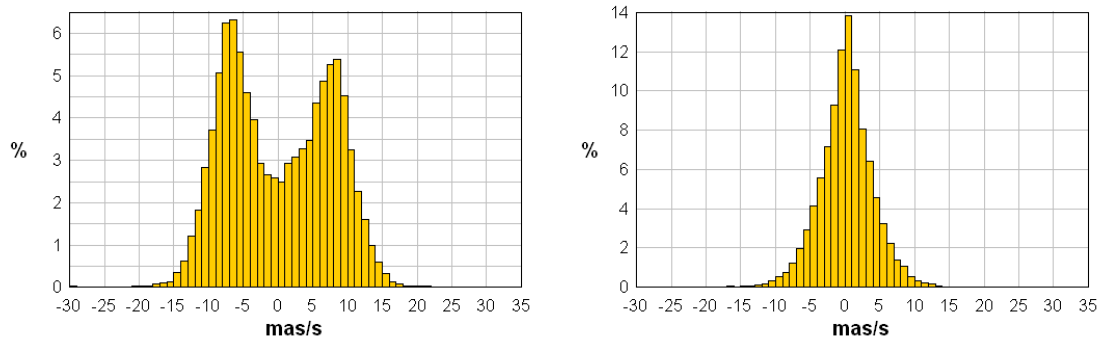


Figure 3: Statistical distribution of the proper velocity of main belt asteroids when they are observed by Gaia. The plots give the along-scan velocity when the observations take place at small solar elongation ($\sim$ 45 deg) on the left panel and at large solar elongation ($\sim$ 135 deg) on the right plot. Velocities are in mas/s.

In addition the two components are not fully independent. At large elongations, when the total speed on the sky is small, the two components tend to be more or less equal (slightly larger for the AC component due to the inclination of the scan circle), while at small angular elongations the across-scan component is always large

(in absolute value). This is very conspicuous in a plot giving the two components for each of the two populations as shown in Fig. 4.

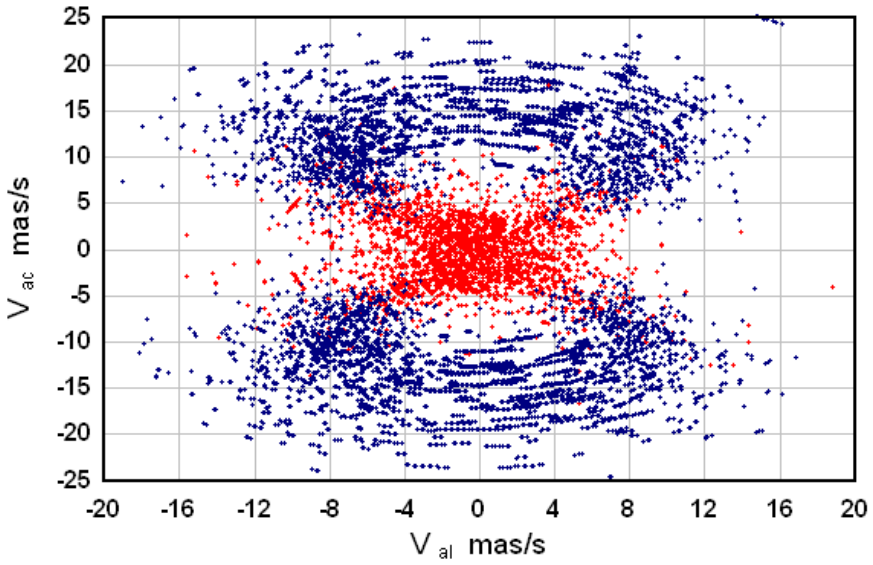


Figure 4: Along and across scan components of the sky velocity for the MBOs at the time they are observable with Gaia. The simulation is based on the first 300 numbered asteroids over 1000 days and one data point (v_{al}, v_{ac}) is plotted for each transit. The small elongations (toward the Sun) are in blue and the large elongations in red.

The velocity distributions for each group of elongations are easily represented with normal distributions and then by combining and properly weighing the different distributions one obtains a very good synthetic representation of the probability distributions of the along and across velocities as,

$$\phi(v) = \sum_{1}^{3} \alpha_i \mathcal{N}(\mu_i, \sigma_i; v) \tag{1}$$

where the relevant numerical values are listed in Table 1 respectively for the along and transverse velocities. The resulting probability density functions are plotted as histograms in Fig. 6. They match quite well the empirical distributions of Fig. 1 based on the simulation, indicating that these distributions can be used with confidence to investigate the windowing effect on the observation of the main belt objects.

The cumulative probability distributions of the speed (the absolute value of the Al and AC components) are plotted in Fig. 7 and will be useful to assess quickly the

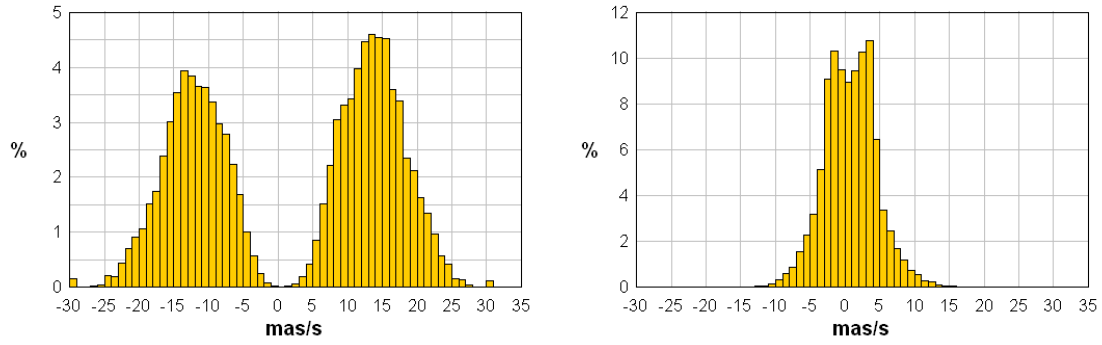


Figure 5: Statistical distribution of the proper velocity of main belt asteroids when they are observed by Gaia. The plots give the across-scan velocity when the observations take place at small solar elongation ($\sim 45\,\mathrm{deg}$) on the left panel and at large solar elongation ($\sim 135\,\mathrm{deg}$) on the right plot. Velocities are in mas/s.

drift in the windows under various assumptions.

In the case of the NEOs two plain centred normal distributions fit the data with $\sigma_{\mathrm{al}} = 22$ mas/s and $\sigma_{\mathrm{ac}} = 30$ mas/s. Finally it will be also useful to represent the velocity distributions of main belt objects with a single gaussian distribution, so that it is easily combined with all the other sources of uncertainty listed by Astrium. In this case on can use for the MBO a centred normal distribution with $\sigma_{\mathrm{al}} = 7$ mas/s and $\sigma_{\mathrm{ac}} = 12$ mas/s, but the approximation is not as good as for the NEOs.

Table 1: Synthetic probability distribution of the along and across-scan velocities of main belt and near earth objects. Each distribution function is a weighted sum of normal distributions as $\sum_1^3 \alpha_i \mathcal{N}(\mu_i, \sigma_i)$ with μ and σ in mas/s.

Objects	V	α_1	μ_1	σ_1	α_2	μ_2	σ_2	α_3	μ_3	σ_3
MBO	along	0.46	0	2.8	0.27	8	3.5	0.27	-8	3.5
	across	0.46	0	4.0	0.27	13	5.0	0.27	-13	5.0
NEO	along	1.0	0	22.0						
	across	1.0	0	30.0						

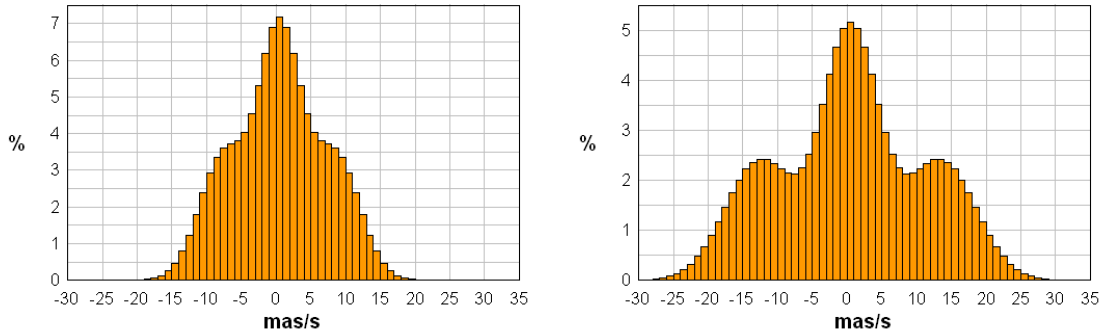


Figure 6: Statistical distribution of the proper velocity of main belt asteroids when they are observed by Gaia. The plots give the along (left) and across (right) scan velocities computed from a weighted sampling of three normal distributions to allow for observations clustering at the two extreme range of allowed elongations. Comparison with Fig. 1 shows that this simple combination of populations provides a realistic model of the velocity distribution.

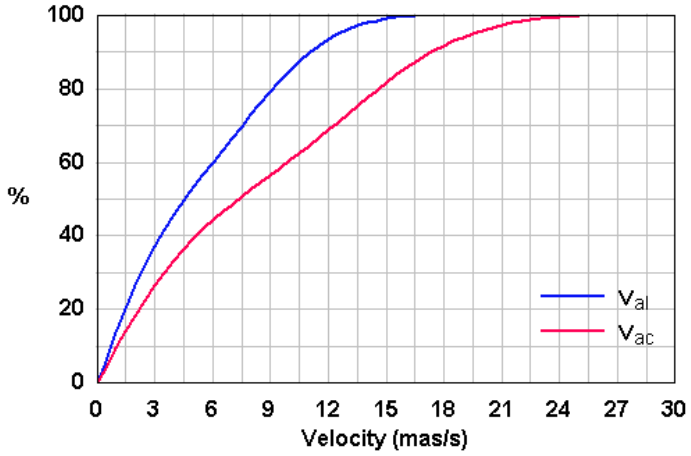


Figure 7: Cumulative distribution of the along and across scan modulus of the velocity for main belt objects during a transit in one of the Gaia FOVs. 87% (resp. 62 %) of the objects have an AL (resp. AC) velocity less than 10 mas/s in absolute value.

3 Observation rate

In case dedicated on-board window handling is implemented for the solar system objects and also for the telemetry budget it is important to have an idea of how

many observations are concerned and how frequently they will occur. The total number of solar system objects observable with Gaia can be safely estimated from the ground-based counts to something close to 500,000. They are definitely not uniformly distributed on the sky, but rather much clustered in the vicinity of the ecliptic. Therefore observations will only occur when one of the two FOVs will cross the ecliptic and the rate of arrival of solar system objects will be rather uneven. Thus there will be a significant modulation over a revolution period of 6h with the crossing of the PFOV and the FFOV each occurring once every 3 hours (at the ascending and descending node) and lasting between 30 mn to 1h according to the inclination of the scan circle on the ecliptic and assuming that the planets are within ± 15 deg from the ecliptic, as demonstrated in Fig. 8. The right histogram gives the statistical distribution in ecliptic latitude of a main belt object when it crosses one of the field of view of Gaia.

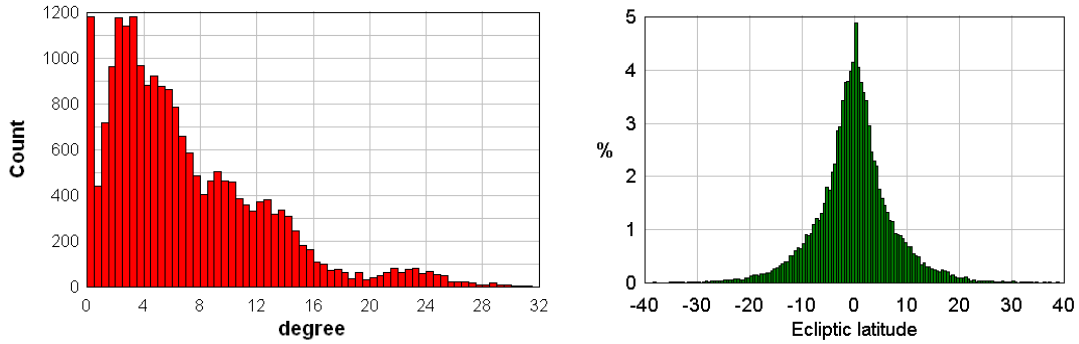


Figure 8: Distribution of the inclination(left) of the orbits of the first 20,000 numbered asteroids and of the ecliptic latitude (right) during a Gaia observation.

At low ecliptic latitude the average number of transits will be of 34 per FOV, giving an average of one source every five seconds entering one of the field (for a total of 500,000 sources). For our simulation on 20,000 sources this leads to about 28 crossings per hour on the average. To quantify the level of fluctuation we have run the simulation over 400 days and counted the number of transits in either field every hour. The statistical distribution shown in Fig. 9 confirms the expected average rate and indicates that the scatter is quite large with 10% of the 1-hour interval with zero to three transits and a significant number of periods with more than twice the average. Finally for the real mission one can adopt the following limits for the number of transits per unit of time of solar system objects in the astro focal plane: from 0 to 30 transits per minute with a modulation primarily determined by the ecliptic latitude of the FOVs. Because of the inclination of the scan circle to the ecliptic, the occurrence of solar system objects transiting at the same time in both

fields will be a rare event.

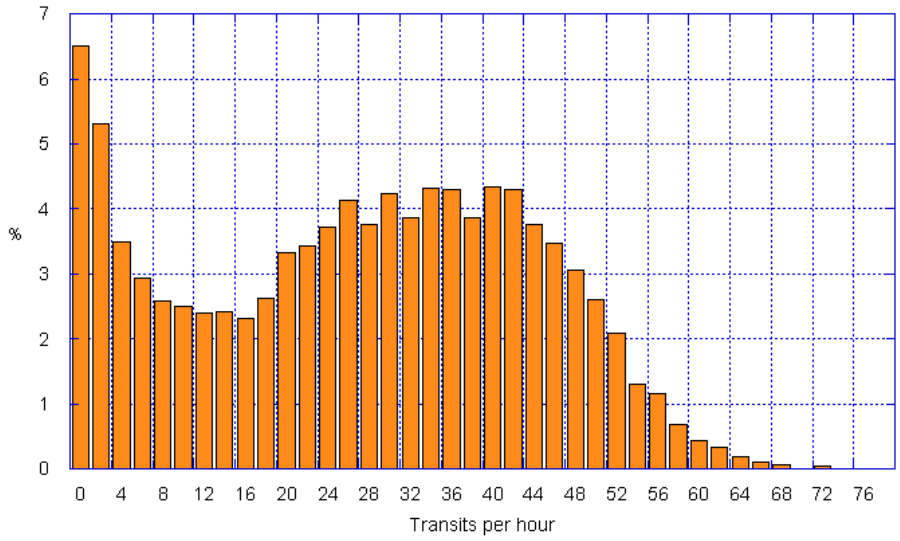


Figure 9: Distribution of the transit rate for MBO. The simulation is based on the first 20,000 numbered asteroids and gives the number of focal plane crossings in number per hour. For the 500,000 observable with Gaia this leads to an average of one crossing every 5 seconds.

4 Survival rate in CCD crossing

4.1 Overall principles

We can now look a the central point of this note, namely the object drifting in the CCD propagated windows. When an object is detected in ASM its crossing time is AF1 is predicted and a check is performed in AF1 to confirm that a source is actually there and that the ASM detection is that of a celestial object. For moving object the prediction of the position will be affected by the motion and, depending on the algorithm, the fastest objects could be outside the predicted area and rejected at this level, although they are observable on the further AFs. This point is not considered in this note and will be reconsidered when a better idea of the algorithm will be available. One should simply notice at this point that with an interval of nearly 11s between ASM1 and AF1, a solar system object with an AL velocity of 20 mas/s will be off the predicted position by more than 3 pixels.

When a window is allocated after the initial location in ASM, the source position in all the AF is predicted using the ASM crossing time and the AOCS information

(both AL and AC displacements from the scanning law are included there). The content of the window is read at the output register of each CCD and processed for transmission. Regarding the latter we have assumed that the transmitted window, when different from the read window, is extracted from an active centring by looking for a peak of counts to select the central sample to be transmitted.

Given the Astrium focal plane layout and for the nominal scan rate we have listed in Table 2 the transit times for the displacement of a star image from the ASM register to the register of one of the astro of photometric CCD. The slight asymmetry between the preceding and following FOV has a non negligible consequences on the survival rate.

Table 2: Time elapsed (in sec) between the register of ASM and the register of an AF or Photometric CCD

FOV	ASM	AF1	AF2	AF3	AF4	AF5	AF6	AF7	AF8	AF9	BP	RP
PFOV	0	10.7	15.5	20.4	25.2	30.1	34.9	39.8	44.6	49.5	56.3	64.1
FFOV	0	5.8	10.7	15.5	20.4	25.2	30.1	34.9	39.8	44.6	51.5	59.3

After the object has been detected in ASM at $t = 0$ (reference time either in ASM1 or ASM2), its position in a moving window at time t is given by,

$$X(t) = vt + st + \delta + \gamma\frac{t^2}{2} \tag{2}$$

where v is the inertial velocity of the planet. The other parameters follow from the Astrium ([3] p. 156) propagation uncertainty model and s denotes the AOCS error between the actual and estimated scan speed, δ the positioning error in ASM and γ the acceleration of the scan motion neglected in the model used to propagate the windows. Therefore for a random planet and for each t_i corresponding to one of the CCD strip, $X(t_i)$ is a random variable. Because the inertial velocity is the largest contributing term it is convenient to write the variance of X as follows,

$$\frac{\sigma^2(X)}{t^2} = \sigma_{\rm v}^2 + \sigma_{\rm s}^2 + \sigma_\delta^2/\delta^2 + t^2\sigma_\gamma^2/4 \tag{3}$$

This quadratic combination of variances applies to each component of the synthetic velocity distribution and contributes to increase the standard deviations listed in Table 1. Using the velocity distribution and the Astrium parameters for the propagation uncertainties one has the values listed in Table 3. The standard deviations for

the AL and AC inertial velocities are indicative, since the probability distribution used is more complex that a single normal law, (see Table 1 for details).

Table 3: Standard deviations of each component of the propagation model. The velocity dispersions are for the MBOs and come from sect. 2.1. The other parameters are from [3] p. 156.

Parameter	AL	AC	unit
$\sigma_{\rm v}$	~ 7	~ 10.5	$\mathrm{mas\,s^{-1}}$
$\sigma_{\rm s}$	2	2.7	$\mathrm{mas\,s^{-1}}$
σ_δ	30	90	mas
σ_γ	0.05	0	$\mathrm{mas\,s^{-2}}$

For a window of width W the condition for the centre of the image to be within the window at time t after the passage in ASM is,

$$|X(t)| < W/2 \tag{4}$$

But this condition is not sufficient to warrant a good retrieval of the astrometric information because when it is just fulfilled half of the image is outside the window and no good statistical estimator can be applied to obtain the image location. One must keep a safety margin to ensure that most of the light in the image is recorded in the read window. The correct condition is then,

$$|X(t)| < W/2 - M \tag{5}$$

where M is the margin at the edge of the window. The margins used are 2 AL pixels in the along scan direction and 1 ac pixel in the transverse direction, primarily needed for the dispersed images. From Eqs. 2-5 and given the PDF of X it is possible to compute the survival rate for various assumptions on the window sizes.

For the along scan motion the probability of this event is then,

$$\mathcal{P} = \int_{-(W/2-M)}^{W/2-M} \phi(x;\sigma(t))\,dx \tag{6}$$

A similar expression holds true in the transverse direction and is included in the following estimates with the corresponding probability distribution and window size. The final success rate is the product of the two probabilities (this assumes that the two components of the velocity are independent, which is not strictly the case as shown in Fig. 4).

4.2 Simulations

Several tools have been used to determine the fraction of the MBO/NEO population which remains observable in the different CCD strips according to the window scheme adopted. An extensive simulation of the crossings in each CCD was run to validate the probability approach. The latter is much easier to use and allows to introduce the propagation uncertainties in the random modelling. The main results are shown below with a set of tables and plots. They give for a set of read windows in AL and AC for each CCD strip the fraction of main belt or NEO sources that enter ASM which are successfully observed in the successive AFs and in BP/RP.

The main assumptions made are:

- Focal plane layout from Astrium design;
- The nominal scanning law is used everywhere to simulate the number of crossing. The transverse velocity arising from the scanning law is assumed to be known at each transit. What is referred here to as the AL and AC velocity is always the extra velocity coming from the orbital motion of the planets.
- Velocity distribution for MBOs and NEOs as described in the previous sections;
- Propagation uncertainty model from Astrium figures with quadratic combination of the errors, without misalignment;
- Along scan images should be within the read window minus 2 AL pixels margins to ensure the recovery of $\sim 80\%$ of the counts;
- In BP and RP the full spectrum must be within the 60 allowed samples.
- Across scan image or spectrum within read window minus 1 AL-pixel (equivalent to a transverse motion limited to 5 AC-pixels with the 12 pix AC-window).
- Active centring is considered: transmitted window are centred on the detection peak with no statistical error. Therefore only the read windows scheme is explored.
- No object is lost by the confirmation algorithm in AF1.

The nominal windows proposed in EHS4 ([2]) is considered in the first exploitation and small variations around this baseline are implemented to assess possible improvements for solar system objects. In particular, without changing the window size, the average number of astrometric observations and the accurate determination of the AL velocity will be improved by using the large window (18 pixels in AL) in AF6 or AF7 instead of AF5, assuming that this choice remains compatible with the

optical quality. By the way the optical center of the system is probably not at AF5 with the current design.

Table 4: Success rate for MBO for AF 1-9 and BP, RP. Read windows are 12 pixels AL (18 for AF 5), 12 pixels AC for AF and photometry. Columns give the survival rate due to Al, AC or for the combined condition.

	PFOV			FFOV		
CCD	AL	AC	AL+AC	AL	AC	AL+AC
1	0.999	1.000	0.999	1.000	1.000	1.000
2	0.970	1.000	0.970	0.999	1.000	0.999
3	0.888	1.000	0.888	0.970	1.000	0.970
4	0.792	1.000	0.792	0.888	1.000	0.888
5	0.952	0.999	0.951	0.987	1.000	0.987
6	0.637	0.991	0.631	0.707	0.999	0.706
7	0.579	0.971	0.562	0.637	0.991	0.631
8	0.531	0.937	0.497	0.579	0.971	0.562
9	0.489	0.893	0.436	0.531	0.937	0.497
10	0.845	0.828	0.699	0.886	0.874	0.775
11	0.781	0.758	0.591	0.820	0.800	0.656

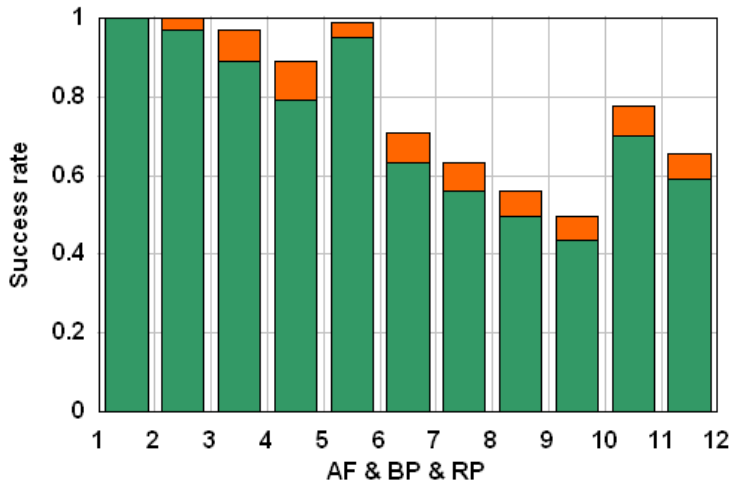


Figure 10: Distribution of the success rate for MBO, PFOV(green) and FFOV (orange) for the baseline window scheme. Read windows of 12 px-AL (18 for AF5), 12 px-AC everywhere. The success rate is computed for each strip of CCD, independently of what happened in the previous.

Table 5: Success rate for MBO for AF 1-9 and BP, RP. Read windows are 18 pixels AL, 12 pixels AC for AF and photometry. Columns give the survival rate due to Al, AC or for the combined condition.

	PFOV			FFOV		
CCD	AL	AC	AL+AC	AL	AC	AL+AC
1	1.000	1.000	1.000	1.000	1.000	1.000
2	1.000	1.000	1.000	1.000	1.000	1.000
3	0.999	1.000	0.999	1.000	1.000	1.000
4	0.987	1.000	0.987	0.999	1.000	0.999
5	0.952	0.999	0.951	0.987	1.000	0.987
6	0.901	0.991	0.893	0.952	0.999	0.951
7	0.843	0.971	0.818	0.901	0.991	0.893
8	0.787	0.937	0.737	0.843	0.971	0.818
9	0.736	0.893	0.657	0.787	0.937	0.737
10	0.845	0.828	0.699	0.886	0.874	0.775
11	0.781	0.758	0.591	0.820	0.800	0.656

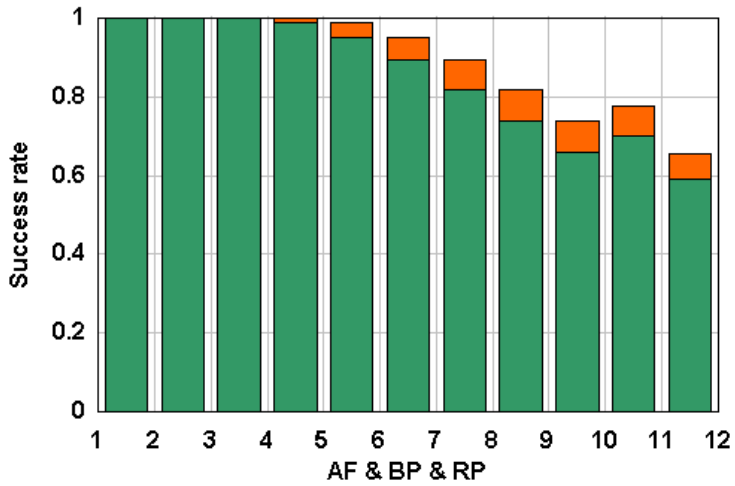


Figure 11: Distribution of the success rate for MBO, PFOV(green) and FFOV (orange). Read windows of 18 px-AL for all AF, 12 px-AC.

Table 6: Same as Table 4 except that a window of 18 AC pixels is used in BP and RP instead of 12. The recovery is significantly better.

	PFOV			FFOV		
CCD	AL	AC	AL+AC	AL	AC	AL+AC
1	0.999	1.000	0.999	1.000	1.000	1.000
2	0.970	1.000	0.970	0.999	1.000	0.999
3	0.888	1.000	0.888	0.970	1.000	0.970
4	0.792	1.000	0.792	0.888	1.000	0.888
5	0.952	0.999	0.951	0.987	1.000	0.987
6	0.637	0.991	0.631	0.707	0.999	0.706
7	0.579	0.971	0.562	0.637	0.991	0.631
8	0.531	0.937	0.497	0.579	0.971	0.562
9	0.489	0.893	0.436	0.531	0.937	0.497
10	0.845	0.991	0.837	0.886	0.997	0.883
11	0.781	0.970	0.757	0.820	0.985	0.807

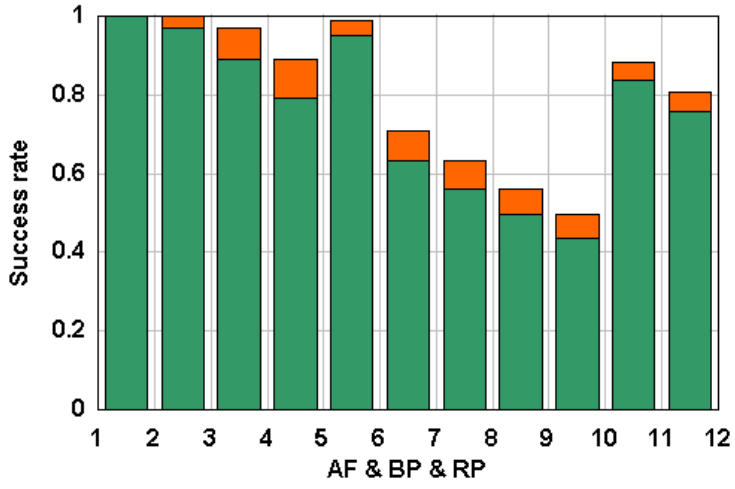


Figure 12: Distribution of the success rate for MBO, PFOV(green) and FFOV (orange). Same as Fig. 10 except that a window of 18 AC pixels is used in BP and RP instead of 12. This allows to recover nearly 80% of all the MBO in the photometric CCDs without active tracking.

Table 7: Success rate for NEO for AF 1-9 and BP, RP. Read windows are 12 pixels AL (18 pixels for AF5) , 12 pixels AC for AF and photometry. Columns give the survival rate due to Al, AC or combined motion. Unlike the MBOs the objects are severly lost in the AC and AL directions.

	PFOV			FFOV		
CCD	AL	AC	AL+AC	AL	AC	AL+AC
1	0.679	0.994	0.674	0.926	1.000	0.926
2	0.506	0.941	0.476	0.679	0.994	0.674
3	0.399	0.850	0.339	0.506	0.941	0.476
4	0.327	0.755	0.247	0.399	0.850	0.339
5	0.465	0.670	0.311	0.540	0.755	0.408
6	0.240	0.599	0.144	0.277	0.670	0.186
7	0.211	0.539	0.114	0.240	0.599	0.144
8	0.189	0.489	0.092	0.211	0.539	0.114
9	0.170	0.447	0.076	0.189	0.489	0.092
10	0.364	0.398	0.145	0.395	0.431	0.170
11	0.322	0.353	0.114	0.347	0.380	0.132

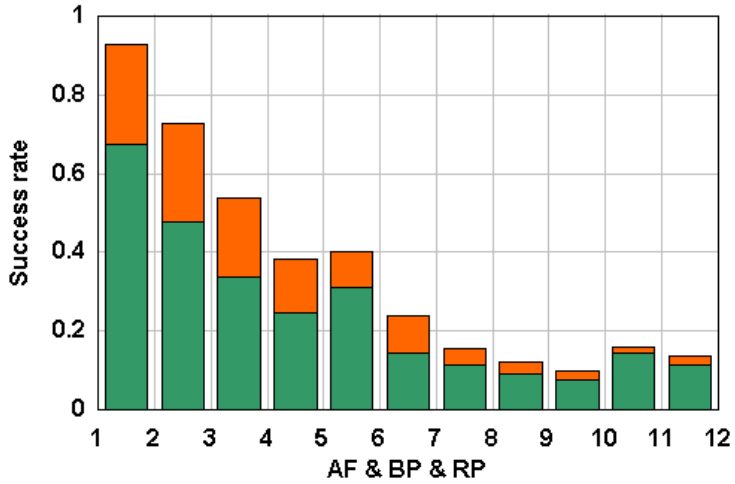


Figure 13: Distribution of the success rate for NEO, PFOV(green) and FFOV (orange). Read windows of 12 px-AL(18 px for AF5), 12 px-AC. There no obvious way to improve the detection without relying to some form of active tracking.

Table 8: Success rate for NEO for AF 1-9 and BP, RP. Read windows are 18 pixels AL for every AF, 12 pixels AC for AF and spectrum. Columns give the survival rate due to AL, AC or combined motion.

	PFOV			FFOV		
CCD	AL	AC	AL+AC	AL	AC	AL+AC
1	0.917	0.994	0.912	0.998	1.000	0.998
2	0.769	0.941	0.723	0.917	0.994	0.912
3	0.639	0.850	0.543	0.769	0.941	0.723
4	0.540	0.755	0.408	0.639	0.850	0.543
5	0.465	0.670	0.311	0.540	0.755	0.408
6	0.406	0.599	0.243	0.465	0.670	0.311
7	0.361	0.539	0.194	0.406	0.599	0.243
8	0.324	0.489	0.158	0.361	0.539	0.194
9	0.294	0.447	0.131	0.324	0.489	0.158
10	0.364	0.398	0.145	0.395	0.431	0.170
11	0.322	0.353	0.114	0.347	0.380	0.132

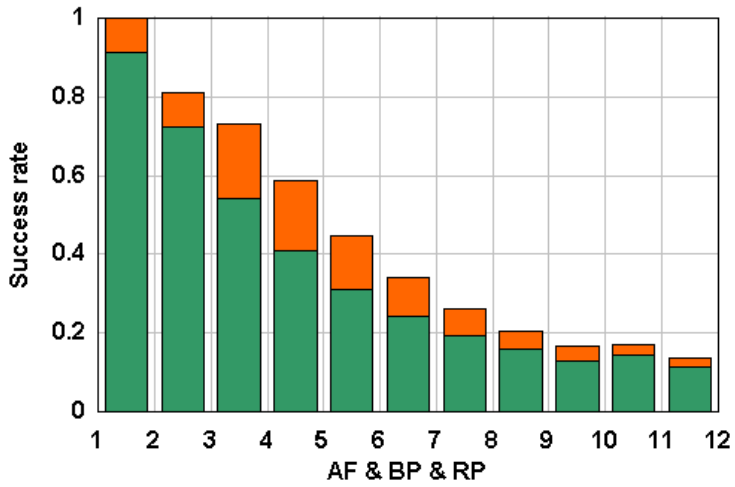


Figure 14: Distribution of the success rate for NEO, PFOV(green) and FFOV (orange). Read windows of 18 px-AL for all AF, 12 px-AC. Slight improvement to Fig. 14 but not satisfactory.

5 How to improve the coverage of moving objects

The survival rates shown in the previous sections indicate already where the effort should be directed to improve the fraction of moving bodies properly observed in the astro and photometric fields. We have looked for possible ways out in a very open way by mentioning solutions that will be quickly ruled out because of their implication on the on board data management. But better to have this discussed once for all and hear from Astrium that some proposals would be very difficult to implement. Basically there are two main directions to investigate :

- larger windows in both directions allowing to maintain most of the MBO sources in the read window, before the useful part in transmitted; to avoid a penalty to the stars, this should be applied only to moving objects after a dedicated test is applied.
- same windows as for the stars, but with an active tracking, taking into account the sky velocity of the sources. This could be applied only to the fastest sources when the nominal windows would fail, while they are good enough for the slowest of the MBOs.

In both cases, as soon as a dedicated window allocation is done only for solar system objects (whatever the mean employed to make the decision), the impact on telemetry is negligible because of the small number of sources involved ($\sim 500,000$).

5.1 Input Catalogue or data uplink

The majority of the moving objects detectable by Gaia after 2012 will have relatively good preliminary orbit from ground based observations. It has been estimated from the current trend of discovery that about 80% of the sources brighter than $V = 20$ will be known by 2012. Knowing the on-board attitude and Gaia orbit and having stored the orbital elements, it is possible to predict rather accurately when a moving object is observed in either field of view, allowing a dedicated window allocation. A similar allocation will be also applied to the fast moving objects based on an internal detection.

To limit the amount of on-board storage and processing, an alternative solution would be to carry out all these calculations on ground and to uplink a sorted observing list, say for about 10 days. The actual duration depends on how well the attitude parameters can be predicted. This limit the on-board handling at the expense of a more complex ground based operations.

5.2 On board velocity detection

The motion is evidenced from the comparison between ASM and AF1, that is to say with a time base of 10.7 s (ASM1) or 5.8 s (ASM2). Even with a positional accuracy as bad as 0.15 pixel in ASM and < 0.1 pix in AF1, this will give detectable velocity at 3σ level as soon as $v_{\rm al} > 3$ or 5.5 mas/s respectively for preceding and following FOVs. This is independent of the knowledge of the AOCS error. The positional accuracy come from [4] but Astrium indicates that this is probably too optimistic at the faint limit and may apply only up to V=18 [5].

Another approach consists of computing for each strip of CCD the maximum along and across velocity which allows the centre of the image of a moving object to be inside the adopted window minus the margin of 2 pixels along and 1 pixel across. For the standard windows the values in mas/s are given in Table 9. So the active window steering to improve the observational coverage of solar system objects is only when the absolute value of either component is larger than the limit of the table. In practice this is only applicable to the AL velocity, since no accurate measurement of the transverse velocity can be done on board. For example to remove the consequences of the AL drift in the photometric CCDs one needs to apply an active steering only if the along scan velocity is larger than 9 mas/s (in absolute value).

There are two different cases to consider :

- For the slow moving objects in the along-scan direction ($v_{\rm al} < 5.5$ mas/s) no dedicated window scheme will be needed. In the worst case the displacement in AF9 will be 150 mas (PFOV) or 250 mas (FFOV), that is to say 2.5 or 4 pixels. Adding quadratically the other propagation uncertainties (~ 2 pix) this yields respectively 3.2 and 4.5 pix. Even in AF9 this can be marginally accommodated with a read window of 12 pixels AL and with full satisfaction with 14 pixels. The 12 background pixels on either side of the low resolution spectra are also sufficient in the along scan direction. This applies primarily to virtually all observations of MBO at large solar elongation (see Fig. 5).

- For velocity larger than 5.5 mas/s (for the AF CCDs) or larger than 9 mas/s (for the BP/RP only), the motion will be recognised from the ASM and AF1 centroiding and this could be used to either adapt the window size specifically for these sources (wider read window) or to implement a dedicated steering. The number of non moving sources falling in this case will be very small ($< 10^6$) with a 3σ testing and will entail no serious impact on the standard processing.

Nothing comparable will be achieved in the transverse direction, and if no precomputed information is available. A good solution would be to enlarge the AC size of

Table 9: Along and across scan sky velocities in mas/s beyond which observations are lost in AF (line 1 to 9) or BP (line 10) , RP (line 11). For a velocity larger than the limit the centre of the image will lie outside the standard windows minus the margins. The transverse velocity due to the scan law is assumed to be accounted for independently. (Windows: AF = 12 px AL (18 px for AF5), 12 px AC, BP/RP: 12 px background on either side, 12 px AC).

	PFOV		FFOV	
CCD	V_{al}	V_{ac}	V_{al}	V_{ac}
1	22.08	82.80	40.47	151.77
2	15.18	56.93	22.08	82.80
3	11.57	43.37	15.18	56.93
4	9.34	35.03	11.57	43.37
5	13.71	29.38	16.35	35.03
6	6.75	25.30	7.84	29.38
7	5.92	22.22	6.75	25.30
8	5.28	19.80	5.92	22.22
9	4.76	17.86	5.28	19.80
10	10.47	15.70	11.45	17.18
11	9.19	13.79	9.95	14.92

the window in BP and RP to something like 18 pixels (Fig. 12), but this may have serious drawback for the stars. The transverse velocity determination will be probably too poor to implement a valuable 3-σ test to set an active tracking of the window. But this remains to be demonstrated and depends on how many non-moving objects will be wrongly assigned larger windows.

For the NEOs, the AL displacement will be easily detected and an active tracking seems the most appropriate response, since the size of the read windows will be much too large to be acceptable. One can see Tables 7-8 that the loss of a NEO during the field crossing owes as much to the AL motion as to the AC. Therefore a good recovery strategy involves a 2D active tracking and a velocity estimate in both directions.

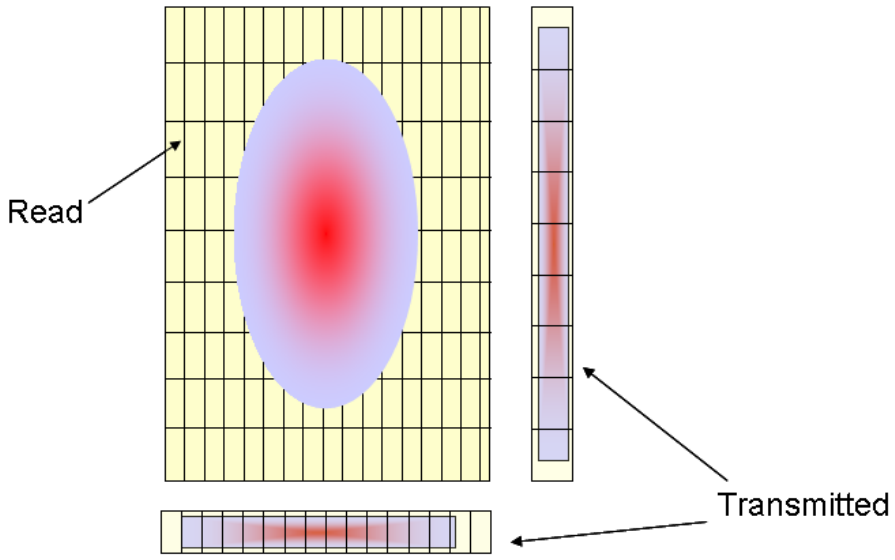


Figure 15: Combination of AL and AC positional information with the binning in both directions and the transmission of two vectors.

5.3 Positional information in the transverse direction

In the course of each transit of a solar system object the positional along scan information will be used to determine the object sky velocity in that direction. However the knowledge of the transverse velocity would be also very desirable for several purposes, like the preliminary orbit determination, the 2D linear orbit extrapolation to thread the observations of a particular object, the prediction of position for ground based follow-up, etc. In many cases this can be obtained with very good accuracy by comparing the transverse position for two successive observations, usually in the preceding and following field. However a significant fraction (about 30%) of the transits will come in isolation because of the large transverse velocity (primarily that coming from the scanning law). A transverse information at one or two pixel level in one of the last astrometric strip (say from AF6 onward) would be a good add-on for the solar system objects. The transmission could be limited to two vectors with the standard AC binning on one hand and an AL binning on the other hand as sketched in Fig.15. The impact on the read-out-noise for stars must be evaluated beforehand, but again this procedure could be limited to low ecliptic latitude.

6 Recommendations

From the above presentation we can set two categories of conclusions :

- the mandatory requirements needed to achieve the basic science with solar

system objects

- the wishes which are options that will improve the science return, but whose introduction is subordinated to the fact that they (i) cause no harm to the other observations (primarily stars), (ii) and they don't add severe complications in the on-board data handling.

R1 Active centring in the read windows must be applied to every solar system source (in practice this means to all detected and confirmed sources)

R2 Velocity estimates carried out for all solar system sources and used to steer the windows in both directions, at least in the BP and RP strips (priority 1) and to the astro CCDs after AF5 (priority 2). The tests should be applied with a safety margin to limit the false positive detection and could be limited to low ecliptic latitude ($|b| < 15\,\mathrm{deg}$).

W1 Displace the large read and transmitted window to AF6 or AF7 instead of AF5

W2 For one strip of CCD (near the end of the astro field) a transmitted vector in the AC direction (that is to say binned in the AL direction) with a 1- or 2-pixel resolution. Would be desirable at every ecliptic latitudes, but acceptable at only low ecliptic latitudes if this is needed to limit the damages to stars.

Acknowledgments

The content of this note has much benefited from discussions with, or comments from, E. Hoeg, F. Arenou, J. de Bruijne and L.Lindegren. They are gratefully acknowledged for their help.

References

[1] Jasniewicz G. et al, 2005, 10th RVS workshop Cambridge September 15-16, 2005 `wwwhip.obspm.fr/gaia/rvs/workshop10Science.html`

[2] Hoeg, E., de Bruijne, J., 2006, Gaia sampling scheme, GAIA-CA-TN-NBI-EH-176-1.

[3] EADS Astrium, 2006, Summary of Gaia satellite design, GAIA.ASF.TCN.SAT.00007.

[4] Arenou, F., 2006, private communication confirmed in a mail on 3 May 2006.

[5] Safa, F., 2006, Communicated at the Instrument Optimisation meeting, held at ESTEC on 4 May 2006.